Nat. Hazards Earth Syst. Sci., 13, 1105–1111, 2013
www.nat-hazards-earth-syst-sci.net/13/1105/2013/
doi:10.5194/nhess-13-1105-2013

Natural Hazards and Earth System Sciences
Open Access

Thermal infrared brightness temperature anomalies associated with the Yushu (China) $M_s = 7.1$ earthquake on 14 April 2010

T. Xie, C. L. Kang, and W. Y. Ma

China Earthquake Networks Center, China Earthquake Administration, Beijing, China

Correspondence to: T. Xie (xtaolake@163.com)

Received: 25 June 2012 – Published in Nat. Hazards Earth Syst. Sci. Discuss.: –
Revised: 26 March 2013 – Accepted: 26 March 2013 – Published: 24 April 2013

Abstract. The paper presents a wavelet transform method to identify possible seismic brightness temperature anomalies that might be associated with the Yushu ($M_s = 7.1$) earthquake that occurred in Qinghai province of China on 14 April 2010. Daily infrared data from the Chinese geostationary meteorological satellite FY-2E were used for the period from 1 January 2010 to 31 December 2011 and the spatial region 28.1–38.1° N by 91.7–101.7° E. We find that the wavelet transform is an effective method to analyse time series which contain nonstationary power, and identify here anomalous power both in the time and frequency domain. The results show that, over the two years, the relative wavelet power spectrum (RWPS) showed anomalous RWPS variations in nine cases: two of these were followed by earthquakes; seven were not. One of the two RWPS anomalies that were followed by an earthquake was in the southern area of the epicentre of the Yushu earthquake, with the RWPS anomaly starting to appear around 29 March 2010, decreasing in the period before the earthquake, and completely gone by 14 April 2010. The Yushu earthquake was the only strong earthquake within the region and two-year time period chosen, so the abnormal change of RWPS during this time period was possibly associated with the Yushu earthquake.

1 Introduction

The dynamic abnormal changes of local thermal infrared (TIR) temperature both in time and space, which were associated with earthquake activities, have been reported by many studies (Gorny et al., 1988; Tronin et al., 2002; Wang and Zhu, 1984; Zhang et al., 2010). Further studies indicated that long-term and successive thermal fields may reflect activities of faults and large liner structure systems in the crust of the earth (Carreno et al., 2001; Ma et al., 2005). Several data process techniques have been introduced and applied to extract possible TIR temperature anomalies caused by earthquake activities of the areas. Intuitively, the transient rise of land surface temperature (LST) may provide us a practical way to detect the TIR anomalies. The phenomenon of strong LST increase of the areas close to epicentre of Gujarat earthquake (India, 26 January 2001, $M_s = 7.9$) appeared before the shock (Ouzounov and Freund, 2004; Saraf and Choudhury, 2005). In order to test credibility of LST increase before Gujarat earthquake, extended LST differencing method based on multiple years of data was used (Blackett et al., 2011). The robust satellite technique (RST), which is based on a statistically well-founded definition of "TIR anomaly", was introduced and applied to studies on the Athens earthquake (Greece, 7 September 1999, $M_s = 5.9$) (Filizzola et al., 2004) and Izmit earthquake (Turkey, 17 August 1999, $M_s = 7.8$) (Tramutoli et al., 2005). A subtraction method was used to work out time series of temperature difference, from which TIR anomalies associated with earthquakes could be picked up (Yang et al., 2010). To choose the reference background temperature which will be subtracted from later temperature images, a model of additive tectonics stress from celestial tide-generating force (ATSCTF) was introduced to select the period in which the background temperature can be chosen (Ma et al., 2012).

The considerations of anomalies associated with seismic activities in the techniques above were directly operated only in time domain. The increase of TIR temperature was regarded as anomalies of the analysed earthquakes. However, other authors have found that careful analyses of data show that the anomalies are just as likely to have an earthquake as not to be followed by an earthquake (Blackett et al., 2011).

The time series of brightness temperature construct signals that contain nonstationary power at different frequencies and at different times. Power spectrum method is an effective way to detect anomalous information in time series. In order to analyse power spectrum anomalies possibly associated with the Yushu earthquake, wavelet power spectrum technique is applied. One merit of wavelet method is its good resolution both in time and frequency domain. Analysed results indicated that, over the two years, relative wavelet power spectrum (RWPS) showed anomalous variations in nine cases. Two of these were followed by earthquakes, while seven were not. The RWPS anomaly for the period from 29 March to 14 April 2010 was in the southern area of the epicentre of the Yushu earthquake. Therefore, the abnormal change of RWPS during this time period was possibly associated with the Yushu earthquake. The rest of this paper is organized as follows. In Sect. 2, we describe some information of the Yushu earthquake and the brightness temperature data to be processed. In Sect. 3, we briefly introduce the wavelet power spectrum technique. In Sect. 4 the brightness temperature anomalies before the Yushu earthquake are described. In Sect. 5 we present a discussion about limitation of brightness data form FY-2E and about RWPS anomalies with no earthquakes that followed. Section 6 concludes the paper.

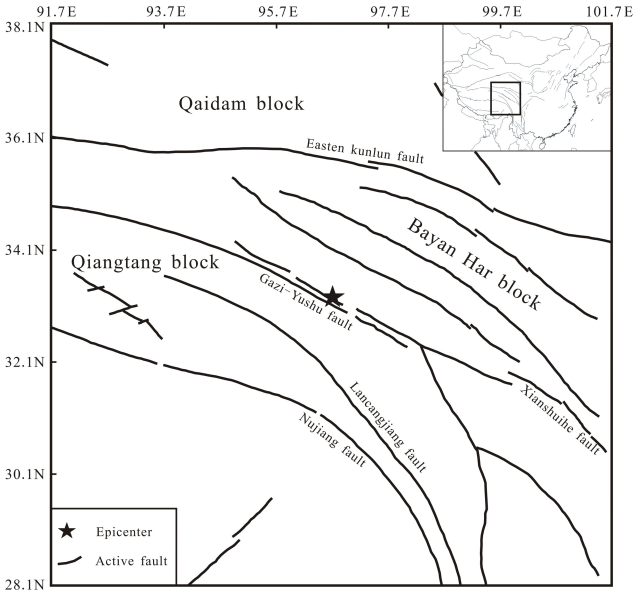

Fig. 1. The epicentre of the Yushu Ms = 7.1 earthquake on 14 April 2010 and main active faults in analysis area (source: China Active Faults.tab, MapSIS Software v. 2011, CEA, 2011). The eastern Tibetan Plateau is divided into several blocks. Eastern Kunlun fault is the boundary of Qaidam block and Bayan Har block. Xianshuihe fault is the boundary of Bayan Har block and Qiangtang block. Great earthquakes mainly occurred at these block boundaries. Seismic activity is relative weak inside blocks (Deng et al., 2003).

2 The Yushu earthquake and brightness temperature data

The earthquake occurred in Yushu county, Qinghai province of China, on 14 April 2010. The location of the epicentre was at 33.2° N and 96.6° E (Fig. 1), and depth was 14 km (CENC, 2010, available at http://www.ceic.ac.cn/). The main shock was rated $M_S = 7.1$ on the surface wave magnitude scale, causing more than 2000 deaths and huge property losses. The earthquake occurred as a result of strike-slipping on a NW–SE left-lateral strike-slip fault named Ganzi-Yushu fault, which is the western segment of the Xianshuihe fault. There were two surface rupture zones caused by the earthquake: one was 31 km in length and the other was 19 km. Xianshuihe fault is a large left-lateral strike-slip fault at the east of the Tibetan Plateau. It starts south of Qinghai province, runs east to west of part of Sichuan province and ends at Yunnan province of China, with more than 1400 km in length. It is the southern boundary of Bayan Har block and the northeastern boundary of Qiangtang block. Xianshuihe fault is an intensive belt of current tectonic deformation and strong seismicity in Tibetan Plateau. Many earthquakes have occurred at this belt in history (Chen et al., 2010).

FY-2E satellite was launched in 2008. Its orbit is fixed at 105° E above the Equator. The entire covering area is 50° N–50° S and 55–155° E. FY-2E began to provide effective data service in November 2009. The resolution of infrared brightness temperature is 5 km. Brightness temperature observation is taken once an hour, and successive data can be obtained. For a certain pixel, the position of satellite and propagation path of thermal radiation is almost fixed. For this reason, data from a geostationary meteorological satellite are used in this paper although the resolution of polar orbit satellite is much better. The spatial coverage of data used in the paper is an area of 28.1–38.1° N and 91.7–101.7° E. Radiations from the sun in daytime can cause increases or relatively sharp perturbs in brightness temperature observed by satellite. To escape effects from solar radiation, the brightness temperature data from 00:00 to 04:00 LT were used in our analysis.

We used the mean of five chosen brightness temperature data as the observed value of this date. Brightness temperature time series with a time resolution of one day were gathered for every pixel. In order to extract information from more frequencies and to analyse anomalies against normality through comparison, the length of daily brightness temperature series was two years. However, some preprocessing needs to be taken on brightness temperature series before using wavelet transform method to detect anomalies. When some pixels were covered by clouds, the brightness temperature of these areas actually reflected temperature of cloudtop. It was much lower than LST under the clouds. We extracted a trend component whose period was about one year and more in brightness temperature of every pixel (e.g. red solid line in Fig. 2a) by using a low-pass filter. A 1.5 times

mean variance threshold (e.g. blue solid line in Fig. 2a) between brightness temperature and its trend component was used to simply eliminate effects of clouds. If the brightness temperature of one pixel is lower than threshold, it was regarded as cloud-top temperature and was substituted with the temperature of its trend component of the same date. Brightness temperature of the pixel after cloud elimination is shown in Fig. 2b.

3 The wavelet power spectrum technique

Wavelet transform is an effective method for analysing nonstationary signal. It is widely used for studies in geophysics, seismic prospecting and other research fields (Kumar and Foufoula, 1997). Wavelet transform is a liner time–frequency analysis method. The conflict between time resolution and frequency resolution can be well solved by changing the shape of time–frequency window. Thus, wavelet transform is localized both in time and frequency domain. The continuous wavelet transform of a signal $f(t)$ is defined as the convolution of $f(t)$ with a scaled wavelet function of $\psi_{a,b}(t)$:

$$W_\psi f(a,b) = \int_{-\infty}^{\infty} f(t)\psi^*_{a,b}(t)\mathrm{d}t, \quad (1)$$

where the asterisk denotes the complex conjugate, and $\psi_{a,b}(t)$ is defined as $\psi_{a,b}(t) = \frac{1}{\sqrt{a}}\psi_{a,b}\left(\frac{t-b}{a}\right)$. a denotes the wavelet scale, and b is the localized time index (Torrence and Compo, 1998). Morlet wavelet is adopted in our analysis. Morlet wavelet consists of a plane wave modulated by a Gaussian in time domain:

$$\psi(t) = \pi^{-1/4} e^{i\omega_0 t} e^{-t^2/2}, \quad (2)$$

where ω_0 is the nondimensional frequency. If $\omega_0 \geq 5$, Morlet wavelet satisfies the admissibility condition, and ω_0 is taken to be 6 here (Farge, 1992). Morlet wavelet is a complex function both in time and Fourier space. Wavelet transform $W_\psi f(a,b)$ is also complex, so the information of amplitude and phase in a certain signal can be obtained. Wavelet power spectrum can be defined as $|W_\psi f(a,b)|^2$. The intrinsic changes of LST vary with the differences of latitude, altitude, climate, etc., which will lead to normal differences in the wavelet power spectrum images. Therefore, RWPS denoted by $R_\psi(a,b)$ is used in our analysis. RWPS is defined as the rate of $|W_\psi f(a,b)|^2$ with the global wavelet spectrum $\overline{W}^2(a,b)$:

$$R_\psi(a,b) = |W_\psi f(a,b)|^2 \Big/ \overline{W}^2(a,b) \quad (3)$$

where $\overline{W}^2(a,b) = \frac{1}{N}\sum_{l=1}^{N} |W_l f(a,b)|^2$, and N is the length of time series.

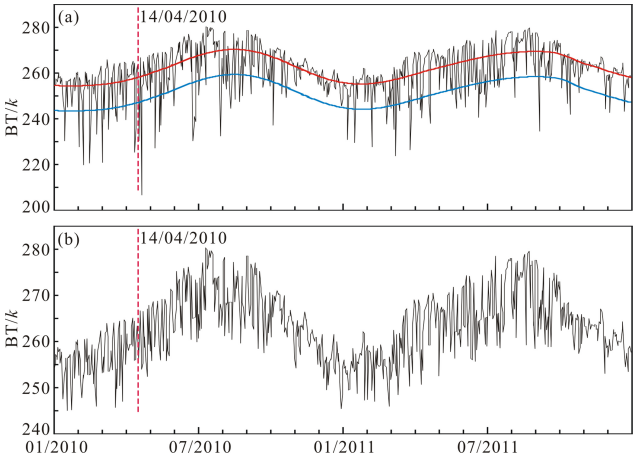

Fig. 2. (a) The raw brightness temperature data of one pixel (5 km × 5 km resolution) was located at 31.8° N, 96.3° E from 1 January 2010 to 31 December 2011. The red solid line is trend component of raw temperature. Blue solid line is 1.5 times mean variance threshold. Temperature below the blue line is seen as cloud-top temperature and is substituted with temperature of the red line on the same date. **(b)** Brightness temperature series after cloud elimination. The high power caused by sharp variations of low cloud-top temperature in power spectrum analysis is removed after cloud elimination. Temperature increase before earthquake often lasts longer than short-time fluctuations. Thus, their power could possibly be presented at different frequencies.

In continuous wavelet transform, discrete spacing of scale factor a determines frequency resolution. The lower discrete spacing of a, and the higher frequency resolution will be obtained. Continuous wavelet method is a nonorthogonal transform. Isolated components of close frequency bands have overlapped information. High frequency resolution is not very necessary, and a is discrete with spacing of 0.5 in our analysis. In time domain, we compute everyday RWPS and localized time index b is taken as 1 here. The length of temperature time series is two years, and N is 730 or 731 as the time interval contains a leap year, in order to show normality against which anomalies might be compared. For a certain frequency band, everyday RWPS of each pixel can be obtained using wavelet transform with coefficients above. We gather RWPS of every pixel on the same date and depict everyday RWPS pictures according to the coordinates of each pixel. It is necessary to note that there are many frequency bands determined by a and N in wavelet transform. However, we focus on the frequency bands between 8 and 64 days in the period (Zhang et al., 2010). Using this method, we can extract and analyse useful information both on time and frequency domain through time–frequency profiles.

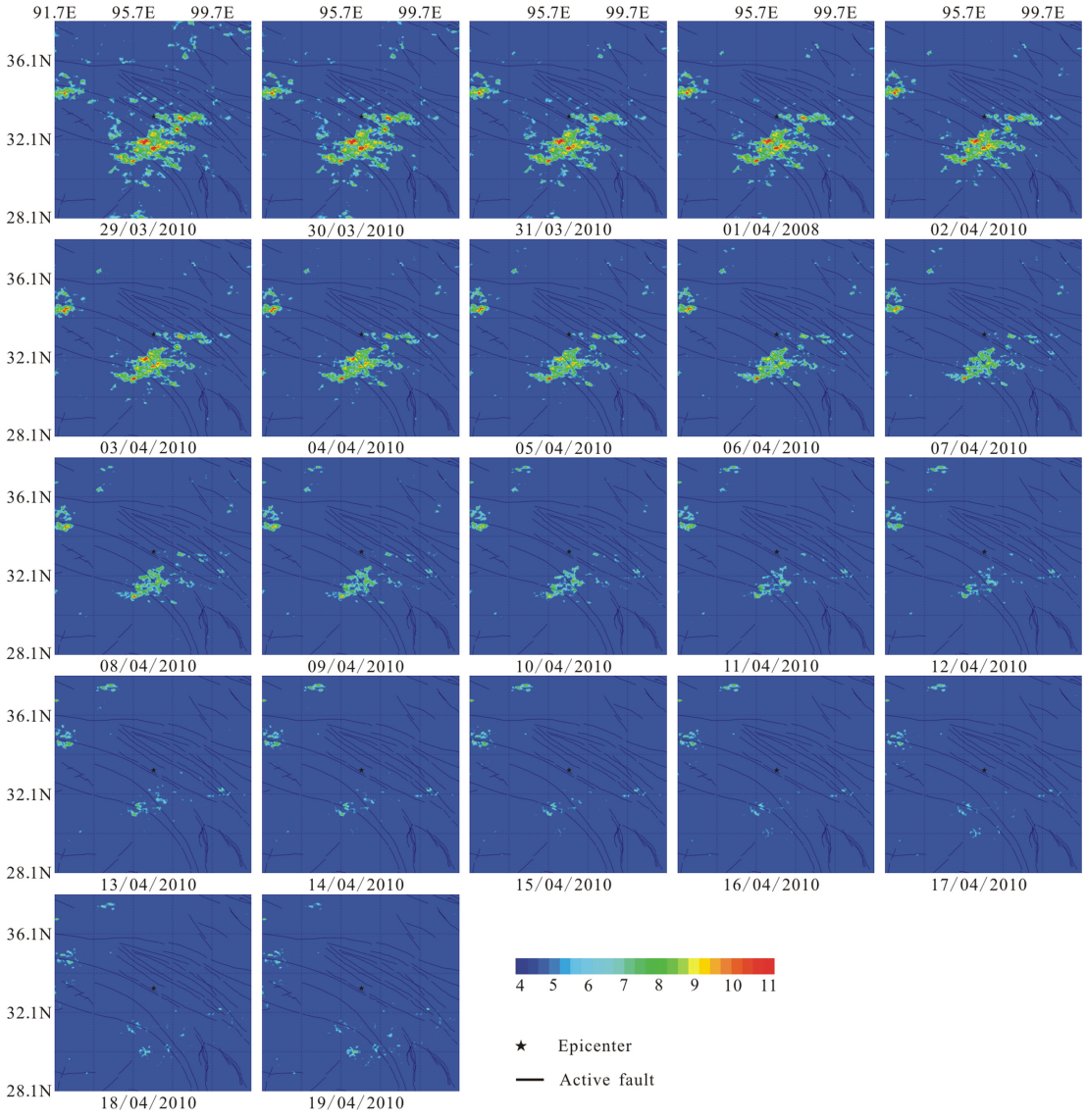

Fig. 3. Spatial-time evolution of the RWPS based on brightness temperature data from FY-2E. For each pixel, value of RWPS means multiples of wavelet power over its average of the two years. Analysed areas are located at eastern Qinghai-Tibetan Plateau. Weather conditions are very complex at different areas, with many short-time fluctuations. Though the power of short-time fluctuations is mainly distributed at high frequency bonds (we focus on RWPS variations whose periods are greater than 8 days), there are still some noise pixels scattered in RWPS images of low frequency bonds. This situation is improved in the analysis of eastern areas of China. The main anomalies are located at the southern areas of epicentre. Anomalous areas and amplitude dwindled and earthquake occurred afterward.

4 The abnormal RWPS changes associated with the Yushu earthquake

The brightness temperature data from 1 January 2010 to 31 December 2011, within the area of 28.1–38.1° N and 91.7–101.7° E, were gathered from FY-2E data service with a spatial resolution of 5 km. We obtained a series of images showing the variations of RWPS in different frequency bands we focused on, using the wavelet method introduced above. Though we have simply eliminated effects of clouds, there were still anomalous pixels scattered in RWPS images. Anomalies possibly associated with earthquakes (or tectonic actions) were identified obeying some rules as follows:

1. The main anomalous pixels should be gathered together, not be scattered in RWPS images.
2. Anomalies should last for days (often more than 10 days).
3. Anomalies must be distributed along tectonic fault zones, especially active fault zones.

We checked RWPS space-time evolution images of different frequency bands and found that an RWPS whose period was 8.26 days displayed anomalous thermal variations before the Yushu earthquake (Fig. 3). It is shown in Fig. 3 that there are conspicuous abnormal RWPS changes close to the epicentre from 29 March to 14 April 2010. The epicentre was located at the northern edge of the anomalous area. In Fig. 3, the epicentre is marked with a black star, and the black solid lines are main active faults in the area.

As is shown in Fig. 3, the abnormal RWPS changes started to appear on 29 March and the spatial abnormal scope mainly appeared in the southern area of epicentre. There were some smaller abnormal areas in the east close to the epicentre. The abnormal area reached a maximum on 29 March and gradually dwindled with time. RWPS amplitude of main abnormal area reached a maximum of about 10, which meant that the power was 10 times its average of two years. Anomaly amplitude also gradually decreased. Since 14 April 2010, the amplitude and spatial scope of anomalies had been so small that it was hard to distinguish thermal anomalies from the background. And anomalies disappeared after the earthquake. Abnormal RWPS reached a peak both in amplitude and scope at the beginning of the whole anomaly evolution and attenuated afterward. This might present a process that LST increased for some reasons in the whole anomaly areas. Then LST dropped and anomalous scope dwindled with thermal diffusion, and returned to normal eventually. Tronin et al. (1996, 2000) suggested that the increase in greenhouse gas (such as CO_2, CH_4) emission rates and the increase of heat flux convection before earthquakes might be the factors causing increase of LST. Another small separate abnormal area was located at the northwest of the epicentre along the same fault, but it is uncertain whether this abnormal area was associated with the Yushu earthquake because the distance from epicentre to the area was more than 400 km.

For better analysing the thermal anomalies associated with this earthquake, a 2 yr RWPS of one pixel (5 km × 5 km resolution, located at 31.8° N, 96.3° E), within our focused bands whose periods are between 8 and 64 days (there are six bonds in our calculation; the period of each band is displayed in Fig. 4), is plotted in Fig. 4 to show normality in other time intervals, against which anomalies can be compared. Before the Yushu earthquake, the values of RWPS whose period was 8.26 days were much higher than those in other time intervals. RWPS of other bands did not show anomalies before the earthquake. In April 2011, the RWPS whose period was 11.7 days exceeded 5, but there were no earthquakes that occurred in the areas throughout that period. The Yushu earthquake was the only strong earthquake within the anomalous areas. Therefore, the conspicuous abnormal RWPS changes of the first frequency band were possibly associated with the Yushu earthquake.

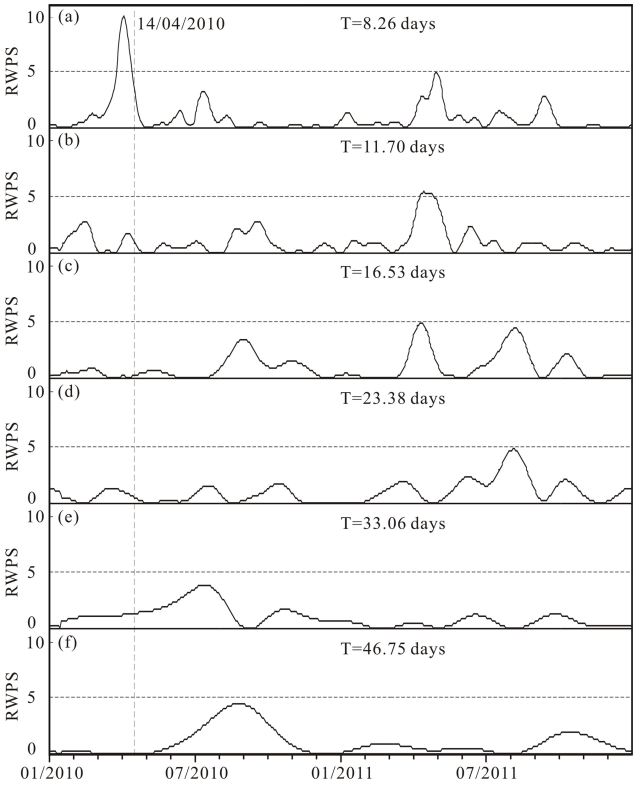

Fig. 4. RWPS of one pixel (5 km × 5 km resolution) was located at 31.8° N, 96.3° E from 1 January 2010 to 31 December 2011. Periods of our focused bands were between 8 and 64 days. If we define RWPS exceeding 5 as anomaly here, there are only two anomalies in the two years. One was in March and April 2010 with a period of 8.26 days (discussed in this paper). The other was in April 2011 with a period of 11.7 days. But there was no earthquake in this anomaly period.

5 Discussion

Brightness temperature data from the geostationary meteorological satellite FY-2E have a high special resolution of 5 km, good time resolution and continuity because the observation is taken once an hour for the whole covering areas. For every pixel, the location of satellite and the propagation path of radiation are approximately fixed. Therefore, brightness temperature and RWPS images can be directly depicted without orbit splicing needed in polar orbit satellite. However, when pixels were covered by clouds, brightness temperature from FY-2E actually reflected the cloud-top temperature which is much lower than land surface temperature under these clouds. Although we can distinguish clouds from satellite cloud images, there is no auxiliary observation to correct brightness temperature of pixels covered by clouds. We simply eliminate cloud using a 1.5 times mean variance threshold in our work, but the effects of clouds on RWPS results still need more evaluations and analyses.

Table 1. RWPS anomalies in the six frequency bands in the selected area during analysis period.

Anomaly	Period	Start date	End date	Latitude range	Longitude range
1	$T = 8.26$ days	10 Feb 2010	6 Mar 2010	31.7–34.8° N	93.0–96.0° E
2		9 Mar 2010	27 Mar 2010	36.5–38.1° N	96.7–101.7° E
3		29 Mar 2010	14 Apr 2010	31.0–33.0° N	95.7–99.5° E
4		23 Jul 2010	13 Aug 2010	28.1–31.0° N	96.7–101.7° E
5		7 Feb 2011	11 Mar 2011	33.0–35.5° N	91.7–93.7° E
6		15 May 2011	6 Jun 2011	28.1–30.0° N	92.0–95.7° E
7	$T = 11.70$ days	6 Mar 2010	26 Mar 2010	36.8–38.1° N	97.0–100.7° E
8		19 Jun 2010	8 Jul 2010	29.0–31.0° N	98.0–99.2° E
9		28 Aug 2011	19 Sep 2011	34.3–37.0° N	95.7–98.0° E
10	$T = 16.53$ days	5 Jun 2010	9 Jul 2010	28.4–30.4° N	96.0–100.0° E
11	$T = 33.06$ days	19 Jun 2010	14 Aug 2010	35.3–38.0° N	96.0–99.0° E
12		10 Jan 2011	23 Feb 2011	33.7–36.0° N	91.7–94.0° E

All works we did above are based on a hypothesis that tectonic actions, especially earthquakes, can cause an increase of LST and its temperature increase lasts longer than short-time fluctuations. Thus, their power could possibly be presented at different frequencies. Though we eliminate many RWPS noises and anomalies unassociated with tectonic actions under the rules in Sect. 4, there are still anomalies within which no earthquakes occurred in the anomalous periods. Among these non-earthquake anomalies, there are at least two situations which we cannot distinguish from our expected anomalies. First, if RWPS anomalies are not caused by tectonic actions but they obey our anomaly identifying rules, they cannot be eliminated. Second, if the anomalies are indeed caused by tectonic actions but no earthquakes occur, we also cannot know if they are non-earthquake anomalies until they disappear. Therefore, we use the RWPS method to extract anomalies obeying the anomaly identifying rules. Fortunately, there are RWPS anomalies before some earthquakes in our case studies.

Table 1 displays RWPS anomalies of each period within our analysis areas from January 2010 to December 2011. A latitude-longitude rectangle was simply used to roughly denote the anomaly area. There are 12 anomalies satisfying the anomaly identifying rules in all frequency bands. However, the anomalies of different frequency bands with duration and area overlapped should be seen as one anomaly. The anomalies numbered 2 and 7 become one, then 5 and 12, and 8 and 10. At last we get 9 anomalies. Table 2 displays all 9 earthquake events with magnitude $M \geq 5.0$ within the area of 28.1–38.1° N and 91.7–101.7° E from 1 January 2010 to 31 December 2011 (http://www.ceic.ac.cn/). If we regard main shock and its aftershocks as one event, there are only 4 earthquake events (actually, aftershocks are not considered in our case studies). The Nierong earthquake occurred about 18 days after anomaly numbered 1 disappeared, while we did not find anomalies before Luhuo and Nangqian earthquakes. Hence, in the whole analysis areas during the period, we find 9 RWPS anomalies with only 2 earthquake events that followed in their anomaly areas, which means 7 anomalies are not associated with an earthquake.

Table 2. Earthquake events in the selected area during analysis period.

Event	Date	Latitude (° N)	Longitude (° E)	Depth (km)	M	Ref. location
1	24 Mar 2010	32.4	93.0	8	5.7	Nierong
2	24 Mar 2010	32.5	92.8	7	5.5	Nierong
3	17 Apr 2010	32.5	92.8	10	5.2	Nierong
4	14 Apr 2010	33.1	96.7	33	7.1	Yushu
5	14 Apr 2010	33.2	96.6	30	6.3	Yushu
6	29 May 2010	33.3	96.3	10	5.7	Yushu
7	3 Jun 2010	33.3	96.3	7	5.3	Yushu
8	10 Apr 2011	31.3	100.9	7	5.3	Luhuo
9	26 Jun 2011	32.4	95.9	10	5.2	Nangqian

6 Conclusions

This paper presents an analysis on the brightness temperature data to identify a possible anomaly associated with the Yushu $M_S = 7.1$ earthquake using continuous wavelet transform method. Over the two years, RWPS showed anomalous variations in nine cases. Two of these were followed by earthquakes, while seven were not. As for the Yushu earthquake, we found that the RWPS whose period was 8.26 days was much higher before the earthquake than the average of the analysed two years. The RWPS anomalies appeared on 29 March. Then the anomalous areas and amplitude dwindled with time, and finally the anomalies disappeared after earthquake. The time-dependent evolution of the RWPS anomalies makes it plausible that "heat" was emitted from the ground at anomalous areas and cooled gradually with time. The Yushu earthquake was the only huge geological event in anomalous areas during the abnormal period, so the conspicuous abnormal RWPS changes were possibly associated with the earthquake.

The wavelet power spectrum technique used in the present paper is an effective method in detecting anomalous variations in a signal. When we use continuous wavelet transform method to analyse a signal in time–frequency domain, we can obtain an RWPS of each frequency band. However, we need to check RWPS images of all bands to extract thermal anomalies that might be associated with earthquakes and other geological events, because the possibly dominant frequency bands of RWPS have not been demonstrated, which will need more earthquake case analyses. On the other hand, there are still anomalies with no earthquakes that followed, which makes false information appear when applying earthquake prediction.

Acknowledgements. The authors would like to acknowledge Satellite Meteorological Center, China Meteorological Administration, for the data service. We thank Matthew Blackett, Bruce D. Malamud, Lixin Wu and an anonymous reviewer for their valuable reviews for improving this manuscript. This work is supported by the project of "Study of anomaly detection and alert techniques based on digital electromagnetic data" (Grant No.: 2012BAK19B02-03).

Edited by: B. D. Malamud
Reviewed by: M. Blackett and L. Wu

References

Blackett, M., Wooster, M. J., and Malamud, B. D.: Exploring land surface temperature earthquake precursors: A focus on the Gujarat (India) earthquake of 2001, Geophys. Res. Lett., 38, L15303, doi:10.1029/2011GL048282, 2011.

Carreno, E., Capote, R., Yague, A., Tordesillas, J. M., Lopez, M. M., Ardizone, J., Suarez, A., Lzquierdo, A., Tsige, M., Martinez, J., and Insua, J. M.: Observations of thermal anomaly associated to seismic activity from remote sensing, General Assembly of European Seismology Commission, Portugal, 265–269, 2001.

Chen, L. C., Wang, H., Ran, Y. K., Sun, X. Z., Su, G. Wu., Wang, J., Tan, X. B., Li, Z. M., and Zhang, X. Q.:: The M_S7.1 Yushu earth quake surface ruptures and historical earthquakes, Chinese Sci. Bull., 55, 1200–1205, 2010 (in Chinese).

Deng, Q. D., Zhang, P. Z., Ran, Y. K., Yang, X. P., Min, W., and Chu, Q. Z.: Basic characteristics of active tectonics of China, Sci. in China (series D), 46, 356–372, 2003.

Farge, M.: Wavelet transform and their applications to turbulence, Annu. Rev. Fluid Mech., 24, 395–458, 1992.

Filizzola, C., Pergola, N., Pietrapertosa, C., and Tramutoli, V.: Robust satellite techniques for seismically active areas monitoring: a sensitivity analysis on September 7, 1999 Athens's earthquake, Phys. Chem. Earth, 29, 517–527, doi:10.1016/j.pce.2003.11.019, 2004.

Gorny, V. I., Salman, A. G., Tronin, A. A., and Shilin, B. V.: The earth's outgoing IR radiation as an indicator of seismic activity, Proc. Acad. Sci. USSR, 301, 67–69, 1988.

Kumar, P. and Foufoula, E.: Wavelet analysis for geophysical applications, Rev. Geophys., 35, 385–412, 1997.

Ma, J., Wang, Y. P., Chen, S. Y., Liu, P. X., and Liu, L. Q.: The relations between thermal infrared information and fault activities, Prog. Nat. Sci., 15, 1467–1475, 2005 (in Chinese).

Ma, W. Y., Wang, H., Li, F. S., and Ma, W. M.: Relation between the celestial tide-generating stress and the temperature variations of the Abruzzo $M = 6.3$ Earthquake in April 2009, Nat. Hazards Earth Syst. Sci., 12, 819–827, doi:10.5194/nhess-12-819-2012, 2012.

Ouzounov, D. and Freund, F.: Mid-infrared emission prior to strong earthquakes analyzed by remote sensing data, Adv. Space Res., 33, 268–273, doi:10.1016/S0273-1177(03)00486-1, 2004.

Saraf, A. K. and Choudhury, S.: NOAA-AVHRR detects thermal anomaly associated with the 26 January 2001 Bhuj earthquake, Gujarat, India, Int. J. Remote Sens., 26, 1065–1073, doi:10.1080/01431160310001642368, 2005.

Torrence, C. and Compo, G. P.: A practical guide to wavelet analysis, B. Am. Meteorol. Soc., 79, 61–78, doi:10.1175/1520-0477(1998)079<0061:APGTWA>2.0.CO;2, 1998.

Tramutoli, V., Cuomo, V., and Filizzola, C.: Assessing the potential of thermal infrared satellite surveys for monitoring seismically active areas: The case of Kocaeli (Izmit) earthquake, August 17, 1999, Remote Sens. Environ., 96, 409–426, doi:10.1016/j.rse.2005.04.006, 2005.

Tronin, A. A.: Satellite thermal survey – a new tool for the study of seismoactive regions, Int. J. Remote Sens., 41, 1439–1455, doi:10.1080/01431169608948716, 1996.

Tronin, A. A.: Thermal IR satellite sensor data application for earthquake research in China, Int. J. Remote Sens., 21, 3169–3177, doi:10.1080/01431160050145054, 2000.

Tronin, A. A., Hayakawa, M., and Molchanov, O. A.: Thermal IR satellite data application for earthquake research in Japan and China, J. Geodyn., 33, 519–534, doi:10.1109/IGARSS.2000.859687, 2002.

Wang, L. Y. and Zhu, C. Z.: Anomalous variations of ground temperature before the Tangsan and Haicheng earthquakes, Journal of Seismological Research, 7, 649–656, 1984 (in Chinese).

Yang, Y. Z. and Guo, G. M.: Studying the thermal anomaly before the Zhangbei earthquake with MTSAT and meteorological data, Int. J. Remote Sens., 31, 2783–2791, doi:10.1080/01431160903095478, 2010.

Zhang, Y. S., Guo, X., Zhong, M. J., Shen, W. R., Li, W., and He, B.: Wenchuan earthquake: Brightness temperature changes from satellite infrared information, Chinese Science Bulletin, Geophysics, 55, 1917–1924, doi:10.1007/s11434-010-3016-8, 2010.